ELSEVIER

International Journal of Pressure Vessels and Piping 75 (1998) 397–415

INTERNATIONAL JOURNAL OF
Pressure Vessels and Piping

Crack-opening-area analyses for circumferential through-wall cracks in pipes—Part III: off-center cracks, restraint of bending, thickness transition and weld residual stresses

S. Rahman[1,*], N. Ghadiali[2], G.M. Wilkowski[2], F. Moberg[3], B. Brickstad[3]

[1]*Department of Mechanical Engineering, The University of Iowa, Iowa City, IA 52242, USA*
[2]*Battelle Memorial Institute, 505 King Avenue, Columbus, OH 43201 2693, USA*
[3]*SAQ Inspection Ltd, PO Box 49306, S-100, 29 Stockholm, Sweden*

Received 31 May 1996; accepted 30 June 1997

Abstract

This is the third of three papers generated from a recent study on crack-opening-area analysis of circumferentially cracked pipes for leak-before-break applications. The first two papers [1,2] [Rahman, S., Brust, F. W., Ghadiali, N. and Wilkowski, G., Crack-opening-area analyses for circumferential through-wall cracks in pipes. Part I—Analytical models. *International Journal of Pressure Vessels and Piping*, (this issue). Rahman, S., Brust, F. W., Ghadiali, N. and Wilkowski, G., Crack-opening-area analyses for circumferential through-wall cracks in pipes. Part II—Model validations. *International Journal of Pressure Vessels and Piping*, (this issue).] dealt with crack-opening-area analysis of pipes assuming simple loading, pipe and crack geometries, and boundary conditions. This paper (Part III—Off-center cracks, restraint of bending, thickness transition, and weld residual stresses) examines several practical aspects of crack-opening-area analysis involving off-center cracks, restraint of pressure-induced bending, girth-weld nozzle cracks at thickness transition, and weld-induced residual stresses. Currently, there are no engineering methods or guidelines available to analyze pipes under these conditions. Both linear-elastic and elastic–plastic finite element analyses were conducted to determine quantitatively their effects on various crack-opening characteristics. From the results of these analyses, recommendations are made on how an off-center crack can be analyzed based on fracture-mechanics equations for a centered crack. It was found when the restraint of bending effects become important and how they should be taken into account. Cracks located in the thickness transition with thickness gradients on both sides of a nozzle girth weld were analyzed. Finally, simplified finite element simulations were performed to determine if the residual stresses should be considered and when they become important for crack-opening evaluations.

1. Introduction

Traditionally, the developments of the crack-opening-area (COA) models have been focussed on idealized conditions for analyzing cracked pipes. For example, it is generally assumed that a simple circumferential through-wall crack exists in the base metal or the weld metal of the pipe with the crack located in the center of the bending plane. The crack-opening area is calculated when this pipe is subjected to remote loads that may include pure bending or pure tension (generally pressure induced) or combined bending and tension. The corresponding analytical models and their evaluations are discussed in [1] (Part I—Analytical Models) and [2] (Part II—Model validations), respectively. In reality, however, the loading conditions, the pipe and crack geometries, and the boundary conditions can be more complicated. For example, the crack in a pipe may become off-centered due to random imperfections around the pipe circumference, or pressure-induced bending may be restrained if the crack is close to a nozzle, or the crack may be located at the thickness transition (e.g. girth-weld crack in a nozzle), or the pipe may have significant weld residual stresses in addition to remote bending loads, etc. Currently, there are no engineering methods or guidelines available to analyze pipes under these conditions. While some of these aspects are applicable to leak-before-break (LBB) analyses, other aspects are more applicable to evaluating flaw stability for a real rather than a hypothetical flaw [3].

The objective of this study is to investigate several practical aspects of crack-opening-area analysis involving off-center cracks, restraint of induced bending from pressure loads, cracks in thickness transition at a nozzle, and weld-induced residual stresses in circumferentially cracked pipes. Both linear-elastic and elastic plastic finite element analyses

* To whom all correspondence should be addressed.

0308-0161/98/$ - see front matter
PII: S0308-0161(97)00083-5

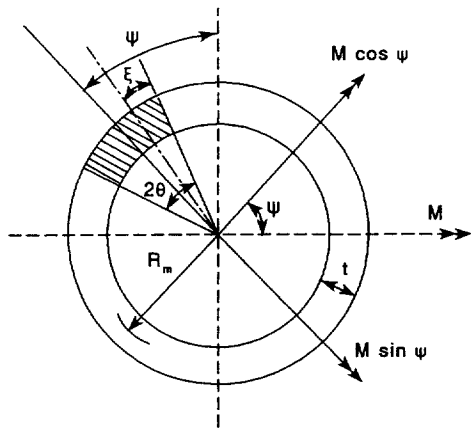

Fig. 1. Pipe cross-section with an off-centered through-wall crack.

were conducted to determine quantitatively their effects on various crack-opening characteristics. From the results of these analyses, recommendations are made on how an off-centered crack can be analyzed based on fracture-mechanics equations for a centered crack. It is found when the restraint of bending effects become important and how they should be taken into account. Cracks located in the thickness transition with gradients on both sides were analyzed. Finally, simplified analyses were performed to determine if the residual stresses should be considered and when they become important for crack-opening evaluations.

2. Off-center cracks

In conducting both leak-rate and flaw stability analyses, a postulated through-wall-crack size (leakage flaw) is often calculated based on its symmetric placement with respect to the bending plane of the pipe [1–3]. This is usually justified with the reasoning that the tensile stress due to bending is largest at the center of this symmetric crack. However, fabrication imperfections will occur randomly around the pipe circumference. Additionally, during the normal operating condition of a plant, the stress component due to pressure is more significant than that due to bending. As such, the postulated leakage flaw may be off-centered and can thus be located anywhere around the pipe circumference, see Fig. 1. Furthermore, a symmetric bending plane under normal operating stresses may be different than the plane under normal plus safe-shutdown earthquake stresses, due to the uncertainty in seismic ground motion. As a consequence, there are two major effects on pipe fracture evaluations:

- For a given leak rate and identically applied load, the detectable flaw size for the off-centered crack will be larger (due to smaller crack-opening area) than that for the symmetrically centered crack (detrimental effect);
- for the same crack length, the load-carrying capacity of the pipe with an off-centered crack will be higher than that with a symmetrically centered crack (beneficial effect).

Since these are two opposing effects, pipe-specific calculations are needed to determine the resultant effect on pipe flaw evaluations. This study examines numerical pipe fracture results to quantify the effects of off-centered cracks on the crack-opening-area analysis of pipes. Both finite element method (FEM) and a simple estimation scheme were employed to compute the center-crack-opening displacement and crack-opening shapes. Recommendations are made on how an off-centered crack can be analyzed based on the analysis of a centered crack and some additional assumptions. Numerical examples are presented to illustrate and support the findings of this study.

2.1. Crack-opening-area analysis of an off-centered crack

Consider a through-wall-cracked (TWC) pipe with mean pipe radius, R_m, wall thickness, t, and through-wall-crack angle, 2θ. The crack is off-centered by an angle, ψ. The pipe and crack geometric parameters are defined in Fig. 1. The pipe is subjected to a pure bending moment, M, without any internal pressure. The stress analysis was linear-elastic, and both plasticity and crack-growth effects were ignored. This is justified since the normal operating stress for typical nuclear piping is well below the yield stress of the material and the relatively short crack being considered should not experience significant crack tip plasticity.

In assessing the crack-opening for an off-centered crack, both finite element and estimation analyses were conducted in this study. They are described below.

2.1.1. Finite element analysis

Standard three-dimensional, linear-elastic, finite element analyses (FEA) were conducted to determine the crack-opening displacement (COD) and the crack-opening shape for a pipe with an off-centered crack. Due to symmetry about loading, only half of the pipe was modeled (Note, symmetry with respect to the crack geometry is violated by the off-centered crack). Since this is a direct method, no further approximations or assumptions are required to evaluate crack-opening characteristics. This is referred to as Method 1 in this paper.

When the crack-opening results are needed for several values of ψ (i.e. for several off-centered cracks), conducting FEA for each of them is not efficient. In this regard, one standard finite element analysis was performed to determine the center-crack-opening-displacement, $\delta(0)$, for a symmetrically centered crack (i.e. when $\psi = 0$) under bending moment, M. Then, the center COD, $\delta(\psi)$, under a bending moment M, for an off-centered crack with angle ψ, was estimated from

$$\delta(\psi) = \delta(0)\cos\psi \tag{1}$$

by resolving the applied moment into its components as shown in Fig. 1. (Note, this is possible due to linear-elastic assumptions). This method will be referred to as Method 2 in this paper. Since no explicit finite element analysis was

conducted for an off-centered crack, exact determination of the crack-opening profile, and hence crack-opening area and leak rate, could not be made by Method 2. In Method 2, it was assumed that the crack-opening shape is elliptical to allow for the computation of the crack-opening area. The justification came from the authors' past studies [4–6] and also from the results of the present study (see Part II paper) [2] which showed that the crack-opening shape for a symmetrically centered crack would approximately follow an elliptical profile. It would be interesting to see how much the crack-opening shape for an off-centered crack would deviate from the ideal elliptical profile [2].

2.1.2. Estimation analysis

For routine fracture calculations, when the finite element analysis cannot be performed or is not needed, the estimation methods discussed in Ref. [2] can also be applied to determine the crack-opening for off-centered cracks. The applications of these methods are similar to Method 2 of the finite element analysis except that the center-crack-opening-displacement, $\delta(0)$, for a symmetrically centered crack is calculated by a suitable estimation scheme. These estimation schemes may include the GE/EPRI method, [7] the LBB.NRC method, [10] the Paris/Tada method, [11] the LBB.ENG2 method, [12] the LBB.ENG3 method [13,14] and others [3,15]. For example, using the GE/EPRI method, the elastic solution of $\delta(0)$ can be obtained from [7–9]

$$\delta(0) = \frac{4R_m^2\theta}{I} V_1^B(\theta/\pi, R_m/t)\frac{M}{E} \tag{2}$$

where I is the moment of inertia of the uncracked pipe cross-section and $V_1^B(\theta/\pi, R_m/t)$ is the influence (elastic) function tabulated in [7–9] for several combinations of θ/π and R_m/t. Note that $\delta(0)$ given above by the GE/EPRI method (and also by other estimation methods) denotes the center COD only at the mid-thickness level, because the elastic V_1 functions, compiled in [7–9] were derived at the mid-thickness of the pipe. See [3,7–9,15] for further details. Similar to Method 2 in FEA, the crack-opening area by the GE/EPRI method can also be approximated by assuming an elliptical crack-opening profile.

2.2. Numerical results

For a numerical example, consider a pipe with outer diameter D_o of 406.4 mm (16 inches), wall thickness (t) of 26.19 mm (1.031 inch), and crack angle ratio (θ/π) of 0.12. The crack is off-centered by an angle (ψ). It is assumed that the crack length is the same on the inside and outside surfaces in terms of percent of pipe circumference. The pipe is subject to a remote bending moment, M = 522.6 kNm (4.626 inch-kip) without any internal pressure. The material behavior is assumed to be linear-elastic. The elastic modulus, E = 193.06 GPa (28,000 ksi) and Poisson's ratio, $\nu = 0.3$ were used.

Linear-elastic finite element analyses were performed for this pipe using the finite-element analysis code ABAQUS [16]. A total of seven analyses were conducted corresponding to the off-centered angles, $\psi = 0$, 15, 30, 45, 60, 75, and 90°. In all cases, 20-noded three-dimensional solid elements were used in the FEA. The total number of elements and nodes were 1260 and 9030, respectively. The number of elements through the thickness was one. Due to symmetry, only half of the pipe was modeled. Fig. 2 shows the finite element mesh for a pipe with an off-centered crack (the shaded region represents the cracked area).

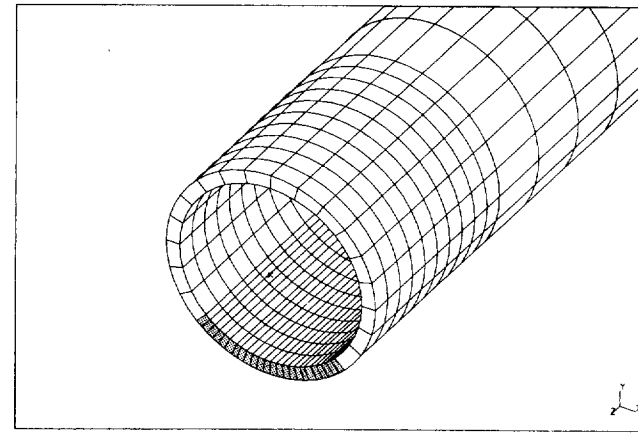

Fig. 2. Finite element model for a pipe with an off-centered crack ($\theta/\pi = 12\%$).

Figs 3 and 4 show the plots of COD vs the normalized coordinate angle, $\xi/2\theta$ representing detailed crack-opening shapes in the inner and outer surfaces of the pipe, respectively, for values of ψ = 0, 15, 30, 45, 60, 75, and 90°. The variable ξ represents an angle from a crack tip and is defined in Fig. 1. The results in Figs 3 and 4 were generated by the direct FEM (i.e. Method 1) described earlier. From Figs 3 and 4, it appears that the maximum COD shifts from the center when the cracks become off-centered. Also, the values of COD for an off-centered crack can become much lower than those for a symmetrically centered crack. Consequently, the crack-opening area (and hence, leak rate) can also be much lower. Hence, idealizing an off-centered

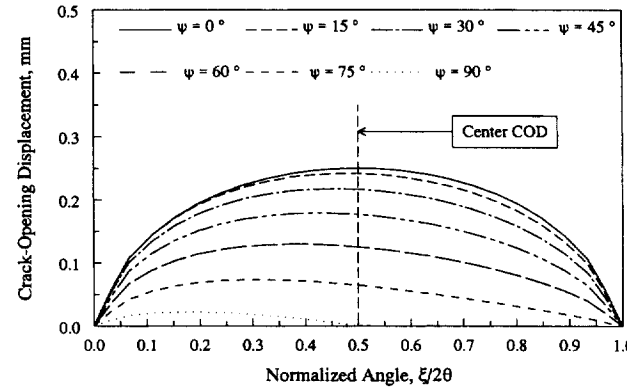

Fig. 3. Predicted crack-opening displacement for various off-centered cracks as a function of $\xi/2\theta$ (inside surface).

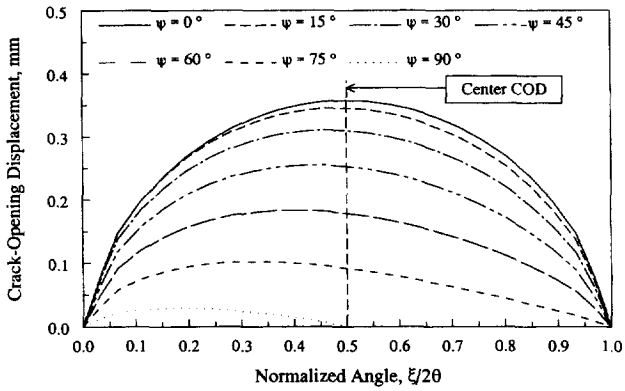

Fig. 4. Predicted crack-opening displacement for various off-centered cracks as a function of $\xi/2\theta$ (outside surface).

crack by a centered crack will yield a smaller crack length for a given leak-rate. The comparison of the results between Figs 3 and 4 show that the COD at the outer surface is larger than that at the inner surface regardless of the value of ψ. Similar results predicting various crack-opening characteristics computed by Method 2 of FEM are shown in Figs 5–8. For comparison, the results from Method 1 are also presented. It appears that the center COD predicted by Method 2 compares extremely well with the corresponding Method 1 solutions. However, the elliptical shape assumed by Method 2 underpredicted the COD for one-half of the crack length and overpredicted the COD for the other half of the crack length (see Figs 5 and 6). But, the comparisons of crack-opening area, which are shown in Fig. 8, reveal that it can be predicted with good accuracy with an elliptical opening profile, i.e. by Method 2. This is an important finding since for leak-rate calculations, accuracy in the prediction of crack-opening area is more significant than that of entire crack-opening shape. This justifies the use of Method 2 of FEM for analysing offcentered cracks in pipe fracture evaluations.

For routine pipe flaw evaluation, when finite element analysis cannot be performed, a suitable estimation method, such as the GE/EPRI method described earlier (see Eq. (2)),

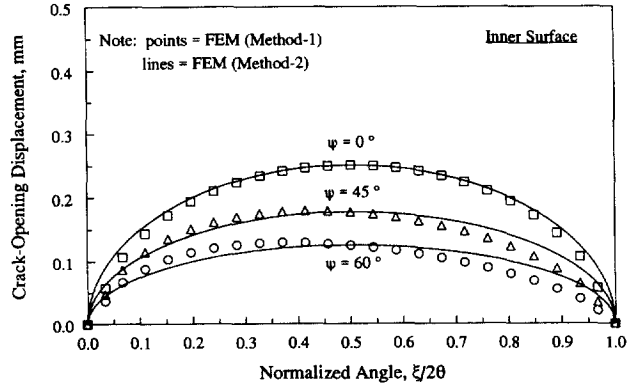

Fig. 5. Comparisons of two finite-element solutions for predicting crack-opening displacement for off-centered cracks as a function of $\xi/2\theta$ (inside surface).

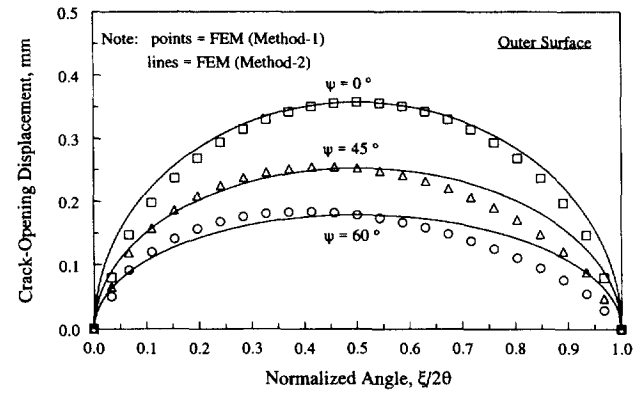

Fig. 6. Comparisons of two finite-element solutions for predicting crack-opening displacement for off-centered cracks as a function of $\xi/2\theta$ (outside surface).

can also be used. Using Eqs. (1) and (2), the predicted center-crack-opening displacements by this estimation method are also shown with the finite element results in Fig. 7. The results of FEM in Fig. 7 are given at the inner, middle, and outer surfaces of the pipe in which the mid-thickness COD was calculated from the average COD values at the inside and the outside surfaces. In the same figure, the estimation results were calculated at the mid-thickness level. The COD solutions by the estimation method compare very well with those from more accurate finite element methods. The comparisons of crack-opening area, shown in Fig. 8, also indicate reasonably accurate predictions by the GE/EPRI estimation method.

2.3. Status of crack-opening methodology

From the numerical results presented in this paper, the effects of an off-centered crack are determined considering only crack-opening area on pipe fracture evaluations. Their effects on the load-carrying capacity and the fracture stability of a leaking crack have not been assessed yet. From a qualitative viewpoint, one can, however, argue that when a crack is off-centered, the crack-driving force, be it stress-intensity factor in linear-elastic fracture or J-integral in

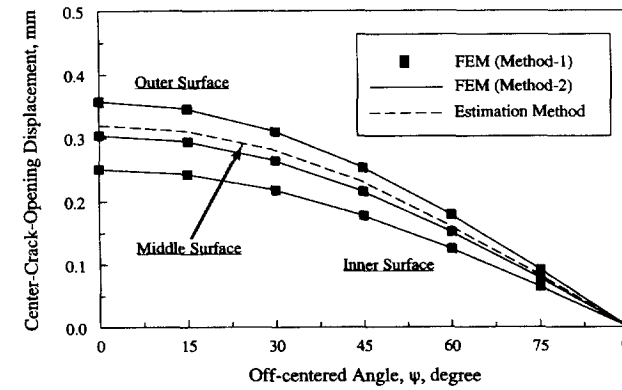

Fig. 7. Predicted center-crack-opening displacement for off-centered cracks by various methods.

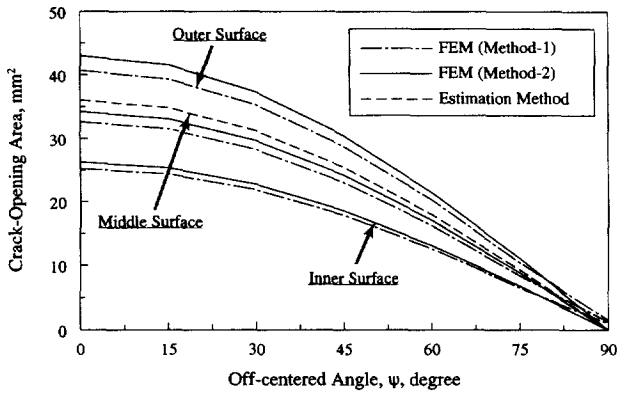

Fig. 8. Predicted crack-opening area for off-centered cracks by various methods.

elastic–plastic fracture, will be lower than that for a centered crack assuming that the bending plane is the same for normal moments and seismic moments. However, it is more likely that these bending planes will differ. Hence, an off-centered crack, which may increase the length of the leakage flaw due to reduced crack-opening, can have positive effects on the maximum load-carrying capacity of pipes. In this paper, the explicit effects on crack-opening area have been quantified. It would be interesting to see how they would be countered by the positive effects related to the structural integrity of the pipes.

3. Restraint of bending from pressure contribution in a pipe system

Current structural analyses for through-wall-cracked pipes subjected to axial tension loads (generally pressure induced) or combined bending and tension loads assume that the pipe is free to rotate. The restraint of the rotation increases the failure stresses, [4,17] but can decrease the crack-opening at a given load. If the pipe system restrains the bending, for example from cracks being close to a nozzle or restraint from the rest of the piping system, then the leak rate will be less than the leak rate calculated by using analyses that assume that the pipe is free to rotate. This will cause the leakage crack size to be larger than that calculated by the current analysis methods for the same leak rate. Since stress due to internal pressure is a significant component of the total stress, this could have a significant effect on the LBB analysis and pipe flaw evaluations. Some scoping calculations were performed to assess the magnitude of the trends.

3.1. Analysis for restraint of axial tension (pressure) induced bending

Fig. 9 illustrates a TWC pipe with mean radius, R_m, wall thickness, t, and an initial through-wall crack angle, 2θ. The pipe is subjected to an axial tension load, P, (due to internal pressure) with full restraint of axial tension (pressure) induced bending at a distance, L_R on either side of the cracked plane. Linear-elastic analyses by the finite element method were performed to examine the effects of restraint due to axial tension-induced bending in a piping system when the pressure load was applied. The results of center-crack-opening displacement as a function of 'restraint length' were investigated. The restraint length (L_R) defined here simply represents the location of the restrained pipe cross-sections from the cracked plane and is shown in Fig. 9.

The following steps were undertaken to determine the effects of restraint of induced bending due to axial tension from internal pressure:

- Step 1—create a finite element model of a cracked pipe with thickness, t, mean pipe diameter, D_m, initial crack angle, 2θ, and total pipe length, $2L_R$ where L_R is the restraint length discussed previously.
- Step 2—apply an arbitrary positive (tensile) displacement loading, Δ, in the longitudinal direction of the pipe to all the nodes in cross-section A-A located (see Fig. 9) at a distance L_R from the cracked plane (i.e. the pipe ends in this case). In this way, the complete restraint of induced bending from tension is simulated symmetrically about the crack. (A non-symmetric restraint analysis would require a more sophisticated model and was not warranted in this initial investigation.)
- Step 3—conduct a finite element analysis and determine the center COD resulting from the remote displacement, Δ. The stresses at the cross-section A-A are not uniform and can be decomposed into a bending component with a linear variation and a tensile component. Denote the center COD (unscaled) and the tension stress by δ_{uns} and σ_{ten}, respectively.
- Step 4—compute the scaled COD, $\delta_s = \delta_{uns} \times (\sigma_{ref}/\sigma_{ten})$, where σ_{ref} is any arbitrarily defined reference tensile stress. The center COD due to a reactive tensile stress, σ_{ref}, with complete restraint of induced bending at cross-sections L_R away from the cracked plane is represented by δ_s. This scaling is permissible due to the linear-elastic stress analysis.
- Step 5—in the same finite element model apply a tension stress loading of magnitude σ_{ref} but allowing free rotation. Denote the resultant center COD by δ_∞, which now represents the reference crack-opening displacement due to an axial tensile stress, σ_{ref}, when there are no external bending restraints present in the pipe, i.e. when the restraint length, L_R approaches infinity.
- Step 6—divide the scaled COD, δ_s, by the reference COD, δ_∞, to get the normalized COD, $\delta_{NOR} = \delta_s/\delta_\infty$. The restrained COD normalized by the unrestrained COD is represented by δ_{NOR}.
- Step 7—for a given crack geometry, repeat steps 1–6 for several values of L_R. Develop a plot of δ_{NOR} vs L_R/D_m and hence, determine the effects of the normalized

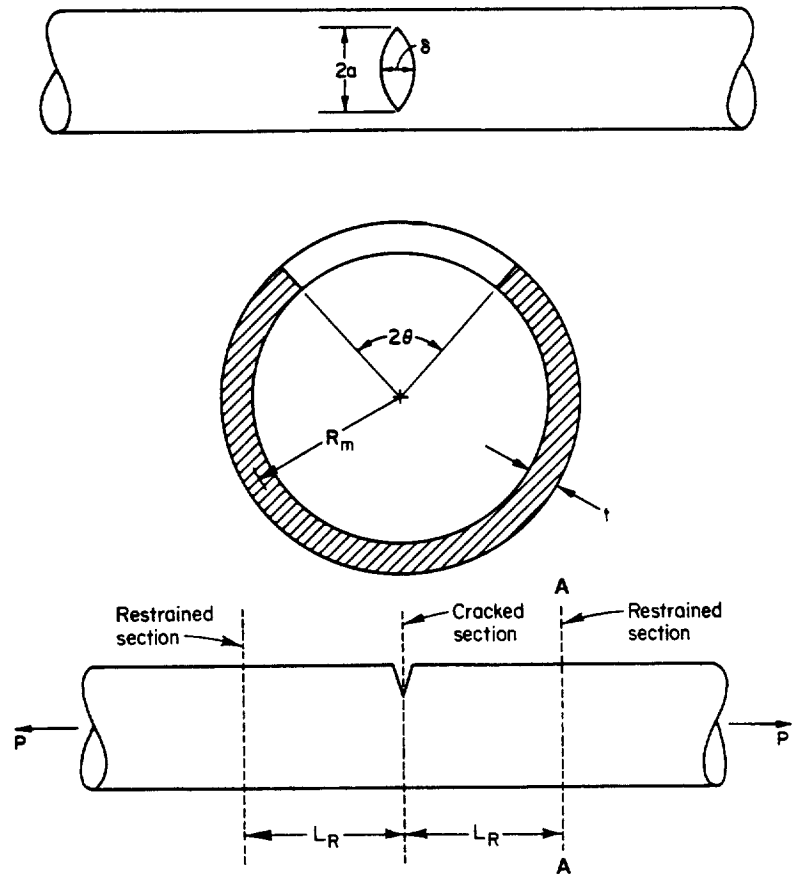

Fig. 9. Schematics of a through-wall-cracked pipe under pure tension (restrained locations prevent rotation and ovalization).

restraint length, L_R/D_m, on the center-crack-opening displacement.

3.2. Numerical applications

As a numerical example, consider a TWC pipe with a mean radius of 355.6 mm (14 inches), thickness of 35.56 mm (1.4 inches), R_m/t of 10, and two distinct cases of initial total crack angles of 2θ where for the two cases $\theta/\pi = 1/8$ and $\theta/\pi = 1/4$ ('small' and 'large' cracks). For material properties, it was assumed that the modulus of elasticity, E, was 200 GPa (29 000 ksi) and Poisson's ratio, ν, was 0.3. The pipe was subjected to remote axial tension as shown in Fig. 9. Linear-elastic analyses by the finite element method were performed using 20-noded three-dimensional solid brick elements in the FEM code ABAQUS [16]. The total number of elements and nodes were 172 and 1252, respectively. The number of elements through the thickness was one. Due to symmetry, only one-quarter of the pipe was modeled. Fig. 10 shows a typical mesh representing the finite element discretization.

Table 1 and Table 2 show the calculated values of various crack-opening displacements for both 'small' ($\theta/\pi = 1/8$) and 'large' ($\theta/\pi = 1/4$) cracks, respectively. These were obtained following the steps described earlier. Several values of restraint length, L_R were considered and are also tabulated. For these calculations, the arbitrary applied displacement, Δ, was set equal to 2.54 mm (0.1 inch) (Step 2). The arbitrary elastic reference tensile stresses, σ_{ref} were assumed to be 849.12 MPa (123.15 ksi) and 650.97 MPa (94.41 ksi) for $\theta/\pi = 1/8$ and $\theta/\pi = 1/4$, respectively (Steps 4 and 5). From the finite element analysis, the corresponding values of reference COD, δ_∞, were computed to be 2.569 mm (0.101 inch) and 8.692 mm (0.342 inch), respectively (Step 5).

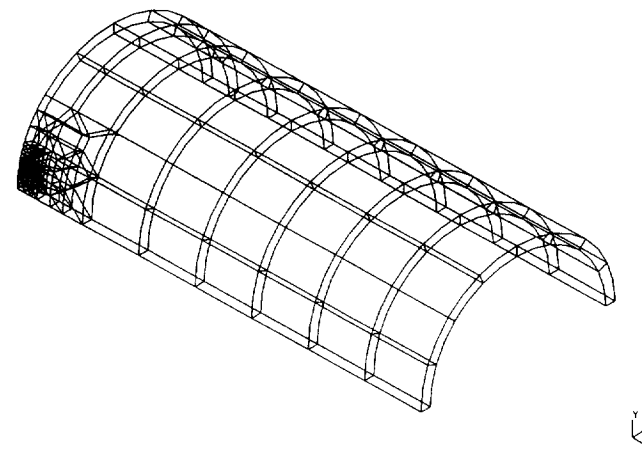

Fig. 10. Finite-element mesh for linear-elastic restraint of crack-opening displacement.

Table 1
Elastic crack-opening displacements for TWC pipe ($\theta/\pi = 1/8$)

$L_R D_m$	Unscaled COD (δ_{uns}) (mm)	Tensile stress (σ_{ten}) (MPa)	Scaled COD (δ_s) (mm)	Normalized COD (δ_{NOR})
1	2.460	849.12	2.460	0.9573
5	0.547	182.47	2.546	0.9909
10	0.290	95.83	2.569	1.000

Fig. 11 presents the results of the calculations for normalized center-crack-opening displacement (δ_{NOR}) as a function of normalized restraint length, L_R/D_m, in which $D_m = 2R_m$ represents the mean pipe diameter. As mentioned before, the COD values are normalized with reference to the crack-opening displacement when there are no external constraints present in the pipe (i.e. when the restraint length becomes infinity), allowing free rotation and ovalization. The results suggest that when the crack angle is small ($\theta/\pi = 1/8$), the restraint effects are also small and may be neglected. However, for larger crack angles ($\theta/\pi = 1/4$), the restrained COD can be significantly different than the unrestrained COD, and hence, should not be ignored in the crack-opening-area analysis for leak-rate quantification. This is especially true for small-diameter pipes in which the leaking crack size for LBB analysis can be large. It is interesting to note that a significant input parameter like the 'restraint length' is not currently considered in either of the thermal-hydraulic codes SQUIRT [5] or PICEP [18] or in any other leak-rate analyses.

3.3. Status of crack-opening methodology

From the numerical results presented so far, the potential reduction of crack-opening area due to the restraint of pressure-induced bending has been evaluated for some specific cases. It is recognized that for a pipe which restrains bending from pressure loads, the load-carrying capacity of the pipe will tend to increase. However, it could be argued that since the normal operating plus seismic loads have a higher percentage of bending than axial membrane loads, the beneficial effects on the fracture loads may not be as great. Nevertheless, the restraint of pressure-induced bending, which may have unfavorable effects on calculating leakage flaw size, can have positive effects on the maximum load-carrying capacity of pipes. In this paper, the effects on crack-opening area have been quantified. It would be useful to also quantify the possible increase in the failure loads and then evaluate how it would counter the effects of crack-opening-area reduction. Hence, further studies and developments are needed to assess quantitatively their resultant effects.

In regard to the effect of restrained bending on failure loads, the following experimental data exists. From one pipe system experiment in the International Piping Integrity Research Group Program (Phase 1), it was experimentally determined that a guillotine break did not occur until the growing through-wall crack was 95% around the circumference [17]. From the pressure loads alone, it was expected that a double-ended guillotine break would occur once the crack reached 65% of the circumference. The 95% crack length corresponded to the pressure-induced failure if the induced bending was restrained. This crack was located 3.4 pipe diameters from an elbow. This is strong evidence of the effect of pressure-induced bending restraint on increasing the load-carrying capacity in a pipe system, even if only at the instability crack length.

4. Circumferential crack at a thickness transition

A practical problem in leak-rate analysis involves evaluating the effects of thickness transition on the crack-opening-area analysis of a circumferential crack. Thickness transition effects can occur, for example, when a crack is postulated at a nozzle girth weld with thickness tapers on both sides with the same or different gradients. Currently, there are no engineering models for calculating crack-opening displacements for such a girth weld nozzle crack. For the case of taper on one side only, one could assume in the limit that the thicker side is infinitely stiff. In that case, the COD at worst is one-half of analysis results using thickness at the thinner side.

This section discusses the analytical efforts undertaken to assess the effects of a typical thickness transition and geometric constraint associated with heavy integrally

Table 2
Elastic crack-opening displacements for TWC pipe ($\theta/\pi = 1/4$)

$L_R D_m$	Unscaled COD (δ_{uns}) (mm)	Tensile stress (σ_{ten}) (MPa)	Scaled COD (δ_s) (mm)	Normalized COD (δ_{NOR})
1	4.873	650.97	4.873	0.5606
5	1.624	174.35	6.065	0.6977
10	0.870	75.84	7.469	0.8593
20	0.474	36.54	8.445	0.9716

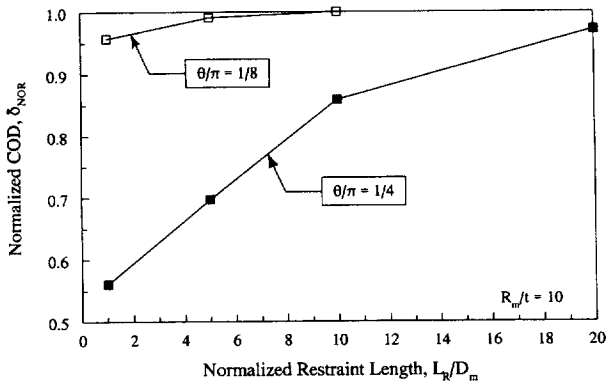

Fig. 11. Effects of fully restrained bending conditions from crack location on COD normalized by unrestrained COD.

reinforced nozzles on the crack-opening displacements for a circumferential through-wall crack in a carbon steel nozzle. This study was conducted to obtain a better understanding of the crack-opening characteristics for circumferential cracks at a thickness transition.

4.1. A girth weld crack at a nozzle with thickness taper

Fig. 12 shows a carbon steel nozzle between a 423.6 mm (16.7 inch) diameter cold-leg pipe and a 333.2 mm (13.1 inch) safety injection line. The outer diameter of the nozzle varies from 534.9 mm (21.1 inches) to 333.2 mm (13.1 inches) with the corresponding wall thickness varying from 124 mm (4.88 inches) to 23.1 mm (0.910 inch). There is thickness gradient on each side of Section D–D as shown in Fig. 12. On one side of Section D–D, the thickness decreases gradually with a constant gradient from 124 mm (4.88 inches) to 46.7 mm (1.84 inches). The gradient is smaller for the other side of Section D–D in which case, the thickness varies from 46.7 mm (1.84 inches) to 23.1 mm (0.91 inch). The thicknesses for the cold-leg pipe and the safety injection line are constant and are equal to 85.1 mm (3.35 inches) and 34.8 mm (1.37 inches), respectively. The geometric properties defining lengths for each of these pipes are given in Fig. 12.

A circumferential through-wall crack was placed in the welded section of the nozzle (i.e. at Section D–D of Fig. 12)

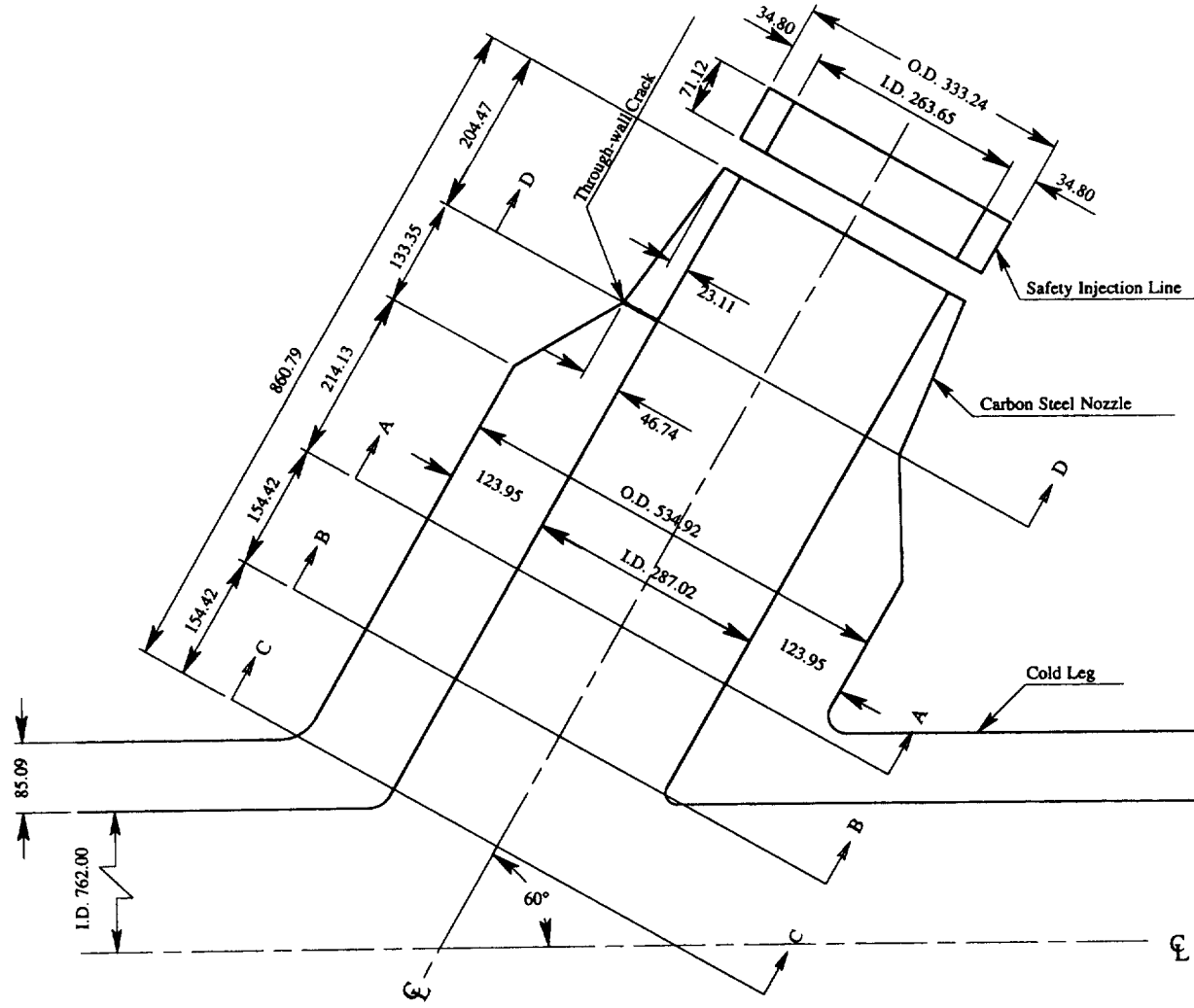

Fig. 12. Geometric details of a carbon steel nozzle with a through-wall crack at thickness transition, dimensions in mm.

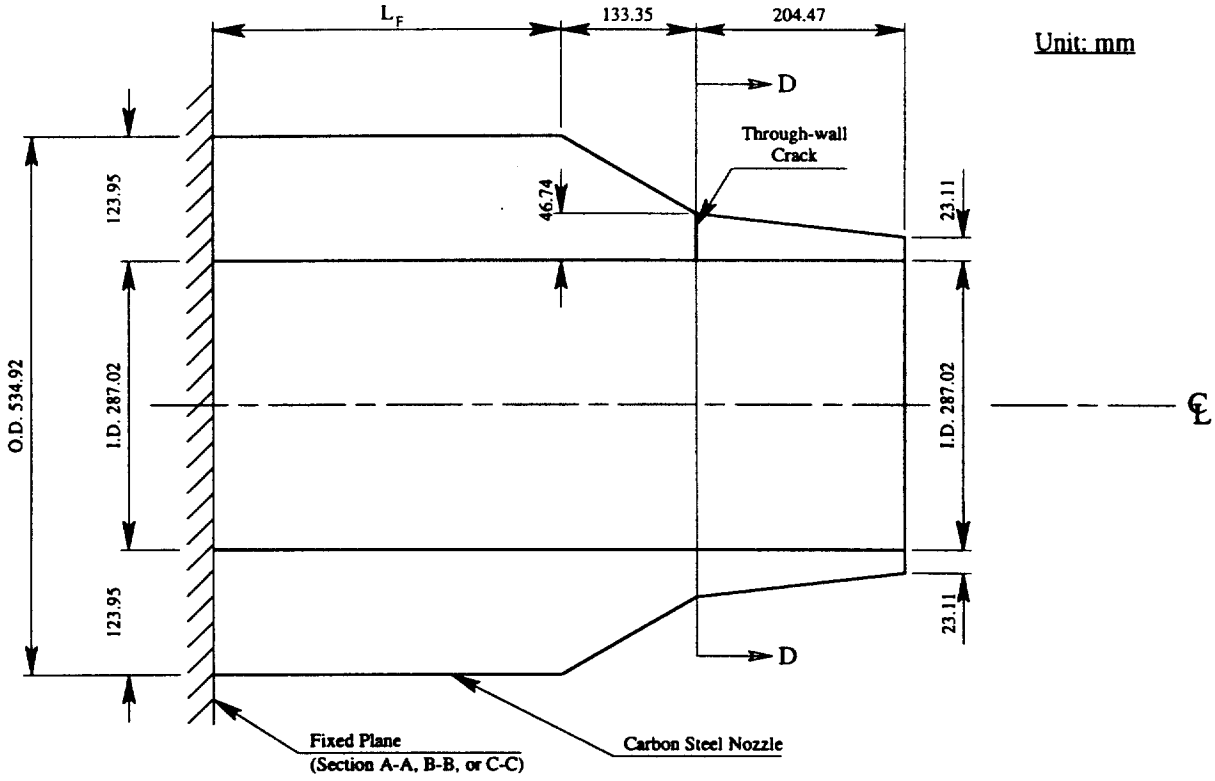

Case 1	L_F = 214.13 mm
Case 2	L_F = 368.55 mm
Case 3	L_F = 522.97 mm

Fig. 13. Idealized nozzle geometry with fixed boundary condition, dimensions in mm.

with thickness gradient on both sides. The crack length was 12.5% of the pipe circumference measured at Section D–D. It was assumed that the crack length on the inside diameter is the same as on the outside diameter in terms of percent of pipe circumference (i.e. the crack tips are radial). The crack was placed in the center of the bending plane of the pipe (i.e. no off-center crack). The crack was assumed to be stationary (i.e. no crack growth).

The material properties of the carbon steel nozzle at 288°C (550 F) are given in Table 3. The values in Table 3 represent the base metal properties of carbon steel. The plastic behavior was represented by the standard Rainberg–Osgood equation (see Eq. (1) of [1]). No weld metal properties were used in the finite element analysis. Also, the material properties of the cold-leg pipe and safety injection line were not used in the analyses.

4.2. Loading conditions

The nozzle was pressurized with an internal pressure of 15.51 MPa (2250 psi) at 288°C (550 F) representing typical operating condition of a pressurized water reactor (PWR). Four different bending moments in addition to the pressure were applied at the free end of the nozzle. The applied bending moments were: $M = 0$ [Load Case 1], $M = 200$ kNm (1770 inch-kip) [Load case 2], $M = 600$ kNm (5311 inch-kip) [Load case 3], and $M = 1000$ kNm (8851 inch-kip) [Load case 4]. For Load Case 1, the pipe

Table 3
Material Properties of carbon steel nozzle at 288°C (550 F) for crack opening analysis

Material properties	Values
Elastic modulus (E), GPa (ksi)	193.1 (28 000)
Poisson's ratio (ν)	0.3
Yield strength (σ_y) MPa (ksi)	237 (34.4)
Ultimate strength (σ_u) MPa (ksi)	610 (88.5)
Ramberg–Osgood coefficient (α)(*)	2.157
Ramberg–Osgood exponent (n)(*)	4.042

(*) The stress–strain ($\sigma - \epsilon$) curve is represented by: $\epsilon/\epsilon_0 = \sigma/\sigma_0 + \alpha(\sigma/\sigma_0)^n$, where $\sigma_0 = \sigma_y$, $\epsilon_0 = \sigma_0/E$.

is under pure tension, whereas for Load Cases 2–4 the pipe is under combined bending and tension with increasing values of moment shown above.

4.3. Finite element analysis

4.3.1. Idealized nozzle geometry

According to Fig. 12, the nozzle has a slanted configuration which makes a full three-dimensional finite element analysis difficult. In addition, modeling the slanted geometry would require large computer resources. To simplify the analysis, an idealized nozzle geometry was chosen and is shown in Fig. 13. The nozzle in Fig. 13 has the same geometric parameters as in Fig. 12 except that one end of the nozzle is completely fixed. The distance between the fixed plane and the nozzle section with largest wall thickness (or outer diameter) is denoted by L_F and is shown in Fig. 13. Due to the uncertainty in the location of this fixed plane, three distinct locations denoted by sections A–A, B–B and C–C and shown in Fig. 12, were considered. Based on the geometric details given in Fig. 12, the values of L_F corresponding to the fixed boundary conditions were:

- Case 1 Boundary Condition (Section A–A)—L_F = 214.13 mm (8.43 inches);
- Case 2 Boundary Condition (Section B–B)—L_F = 368.55 mm (14.51 inches);
- Case 3 Boundary Condition (Section C–C)—L_F = 522.97 mm (20.59 inches);

All three boundary conditions were used in the finite element analyses to determine the effects of L_F on COA as opposed to full three-dimensional analysis of the nozzle and the cold-leg pipe. For the analyses, the moments were applied at the free-end of the idealized nozzle in Fig. 13.

4.3.2. Finite element modeling

Standard three-dimensional, elastic-plastic, finite element analyses were performed for the nozzle pipe in Fig. 13 using the finite-element analysis code ABAQUS [16]. A total of twelve finite element analyses were conducted for four different loading conditions and three different boundary conditions defined earlier. In all cases, 20-noded, three-dimensional solid elements were used in the finite element model. Due to symmetry, only half of the pipe was needed to be modeled. The total number of elements and nodes were 260 and 2093, respectively. The number of elements through the thickness was three. Fig. 14 shows a finite element mesh for half of the nozzle (undeformed configuration) with a crack at the thickness transition.

The ABAQUS analyses were performed using two load steps. The first load step consisted of an internal pressure of 15.514 MPa (2250 psi) applied to the inside of the pipe and also an equivalent tension load due to pressure at the end was applied. In this way, both the axial and circumferential (hoop) stress in the pipe due to internal pressure were

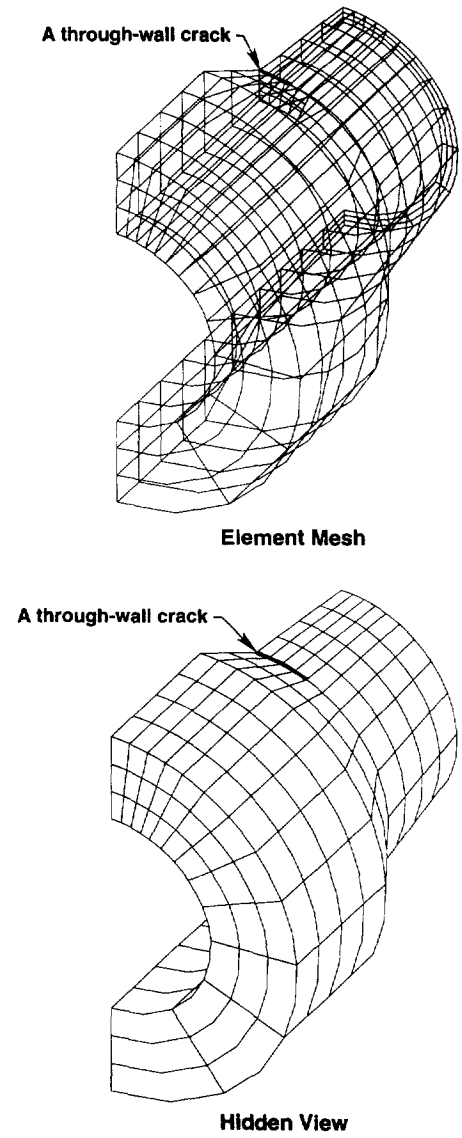

Fig. 14. Finite element model of a carbon steel nozzle with a through-wall crack.

simulated. The second load step consisted of bending moments applied in several substeps up to a maximum of 1.00 MNm (8851 inch-kip).

4.3.3. Results of analysis

Fig. 15 shows the sensitivity of FEM results to the fixed locations defined by the Sections A–A, B–B, and C–C. From this figure, the center-crack-opening displacements calculated at the inner and the outer surfaces of the pipe subjected to two extreme loadings (one was pure pressure and other was combined pressure and bending of 1.00 MNm [8851 inch-kip]) do not appear to be dependent on length, L_F, which defines the location of the fixed plane. Clearly, the crack-opening results are not affected by the choice of the boundary conditions defined earlier. This also implies that the analysis of an idealized nozzle geometry shown in Fig. 13, instead of modeling the combined nozzle and

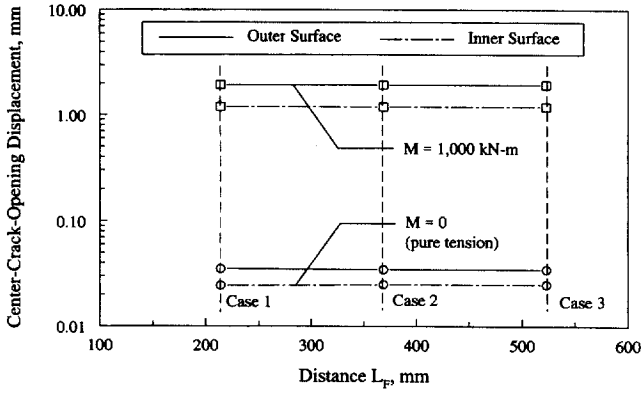

Fig. 15. Center-crack-opening displacement versus location of fixed plane for various applied moments.

cold-leg pipe of Fig. 12 is a useful simplification for crack-opening-area analyses.

Fig. 16(a)–(d) provide detailed plots of crack-opening displacement vs normalized distance from the crack-tip for four different load cases showing the crack-opening profiles of the nozzle crack. For better understanding of the problem, the components of the COD in the direction of both thinner and thicker sides of the cracked section are shown. The 'zero' horizontal lines in Fig. 16 simply denote a straight line joining two crack tips at the deformed configuration of the pipe. A positive value of the COD denotes the component of COD in the thinner side of the crack, whereas a negative value of the COD denotes the component of COD in the thicker side of the crack. Both components of the COD were calculated at the inner and outer surfaces of the pipe from the finite element analyses and are presented in Fig. 16. The results indicate that due to thickness gradient on both sides of the crack, the component of COD in the thinner side is much larger than that in the thicker side, thereby breaking the symmetry of the crack-opening profile about the crack length. The differences in these COD components can be significant when the applied moment is large, e.g. when $M = 1.00$ MNm (8851 inch-kip), see Fig. 16(d).

Finally, Fig. 17 shows the variations of center-crack-opening displacement as a function of the applied moment which are calculated at both inner and outer surfaces of the pipe. The results suggest that the crack-opening behavior is still linear at $M = 600$ kNm (5311 inch-kip), but can be significantly non-linear after that moment is exceeded. This strong non-linearity is clearly exhibited when $M = 1.00$ MNm (8851 inch-kip). The results in Fig. 17 also reveal that there are significant differences in the center CODs at the inner and outer surfaces of the pipe,

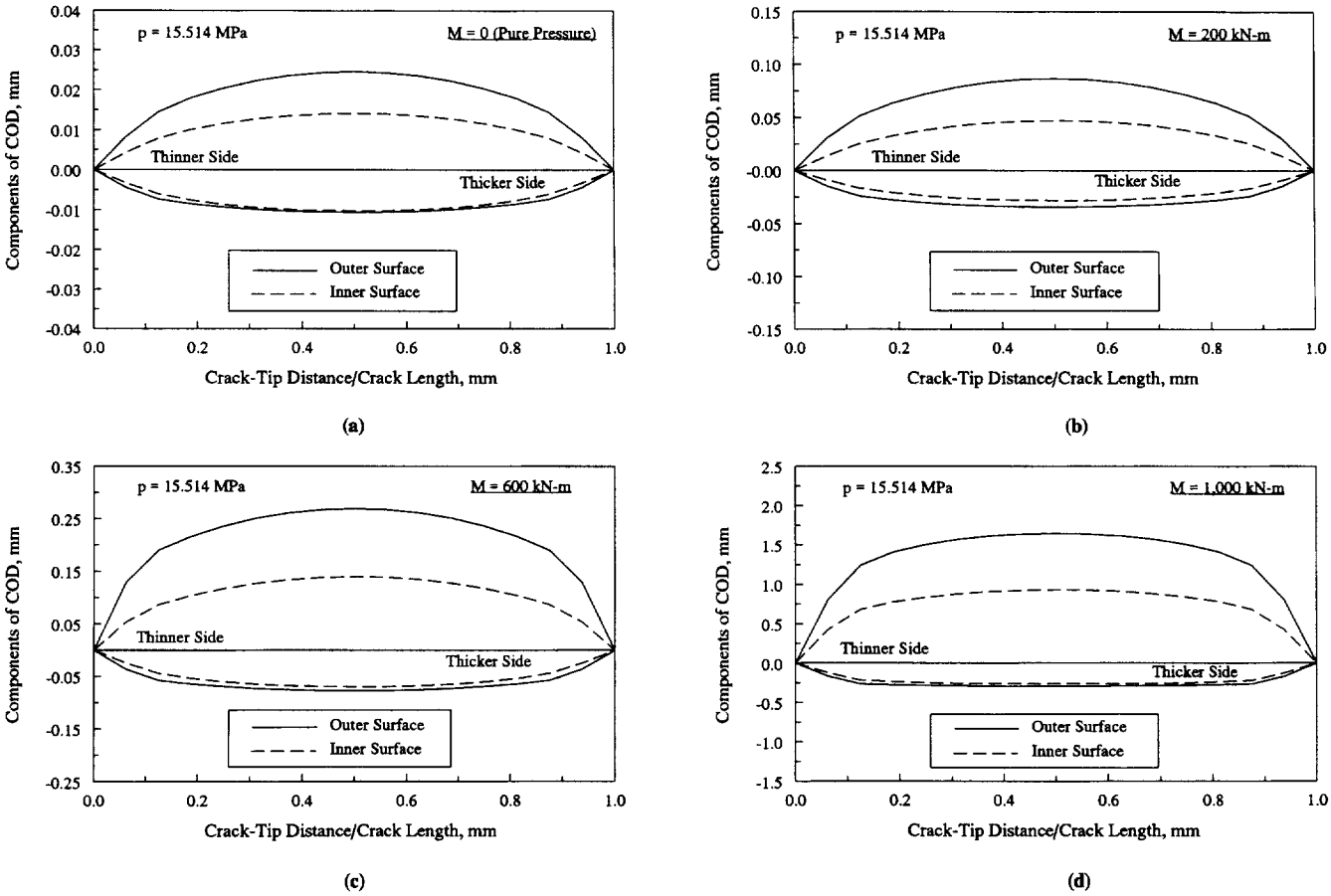

Fig. 16. Crack-opening profiles for: (a) $M = 0$; (b) $M = 200$ kNm; (c) $M = 600$ kNm; and (d) $M = 1000$ kNm.

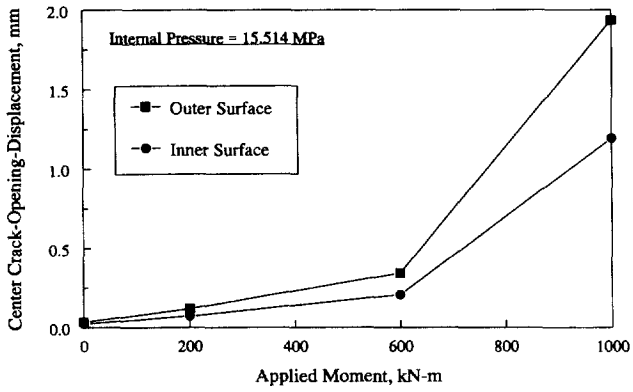

Fig. 17. Center-crack-opening displacement as a function of applied bending moment.

particularly when the applied moment is large. Similar trends were also found for the overall crack-opening shapes which are shown in Fig. 16.

Fig. 18 shows a plot of center-crack-opening displacement (half) vs wall thickness for a straight pipe without any thickness gradient which has the identical crack size, material properties, and inside diameter of the carbon steel nozzle defined earlier. This plot was developed by performing simple linear-elastic analyses by the GE/EPRI method [7–9] for this pipe that was subjected to a bending moment of 200 kNm (1770 inch-kip) and an internal pressure of 15.51 MPa (2250 psi) for several values of wall thickness. The elastic influence functions in the GE/EPRI method were obtained from Ref. [7]. According to the results in Fig. 16(b), the components of center COD (average) in the directions of thinner and thicker sides are 0.067 and 0.031 mm, respectively. Using these finite element results in Fig. 18, the equivalent thicknesses of a pipe without any taper would have to be 44.8 mm (1.76 inches) and 84.0 mm (3.31 inches) to match the components of the center-crack-opening displacement at the thinner and thicker sides of the carbon steel nozzle, respectively. The corresponding ratio of the effective thickness of a constant thickness pipe to the thickness of the nozzle at cracked plane

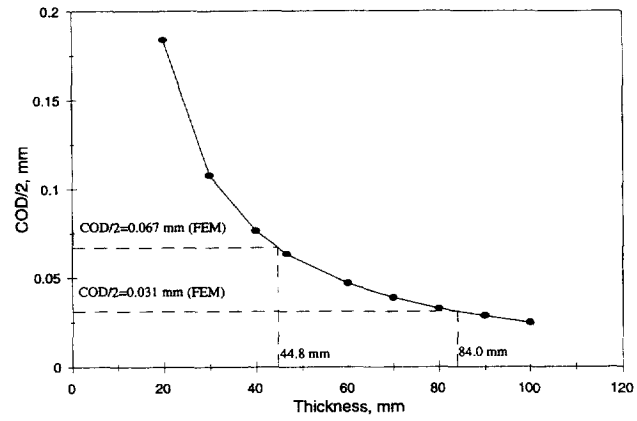

Fig. 18. Crack-opening displacement for a pipe with constant thickness and same inside pipe diameter.

would be 0.96 and 1.8, respectively. Using these ratios, one can then determine the crack-opening for a nozzle crack by conducting simple estimation analyses of a straight pipe without any thickness gradient. However, for general nozzle analysis (elastic), these ratios depend on the angle of taper on either side of the crack, crack size, and possibly, the R_m/t ratio at the cracked plane. To determine the functional relationship between these ratios and the above geometric parameters quantitatively, one would require several finite element analyses by varying these parameters. Hence, further studies are needed to develop a simplified analysis procedure so that the nozzle crack case can be analyzed using simple constant-thickness pipe estimation methods.

5. Effects of residual stresses on crack-opening area

The effect of residual stress on crack-opening displacement (COD) in leak-rate analyses is not well understood. There are no simple analyses to account for those effects and therefore, they are frequently neglected. One objective of this study was to assess the magnitude of the residual stress effects on the crack-opening displacement. The effects of residual stresses are most pronounced on the crack-opening variations through the thickness. The thermal-hydraulic models can account for the effects on leak-rates due to the differences in COD on the inside and outside surfaces of the pipe [5]. The leak-rate aspects of these differences are discussed in Ref. [5]. In this study, standard linear-elastic, finite element analyses were conducted to compute the crack-opening displacement for a pipe with and without residual stresses.

5.1. Simulation of residual stresses

Attempts to understand the effects of weld parameters on residual stresses have been made through experimentation by various researchers at Battelle [19–23], General Electric [24], Argonne National Laboratory [25–27] and others [28–34]. A computational model for predicting residual stresses due to girth welding of pipes has also been developed [19–23]. This model, verified with past experimental data, usually involves two parts: (1) a temperature model; and (2) a thermal stress model. The temperature analysis is based on the steady-state heat flow due to a point source moving at a constant speed in an infinite solid. The thermal stress model is an axisymmetric finite element analysis which allows temperature-dependent material properties and elastic unloading. The output from the thermal analysis consists of the temperature vs time histories in each finite element for each individual pass. These temperature histories then provide the input for the finite element analysis to compute stresses and strains in the body. In this way, the weld residual stresses in a pipe can be accurately simulated.

The computational approach, defined above, involves

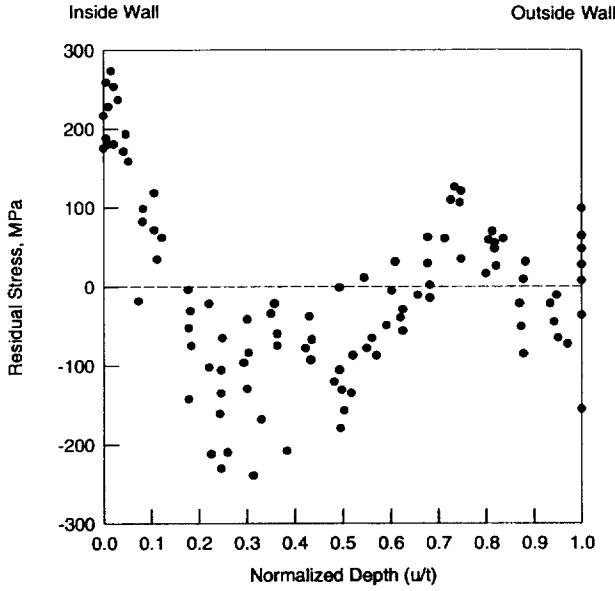

Fig. 19. Measured axial through-wall residual stress as a function of radial distance through the pipe wall for austenitic stainless steel pipe welds.

comprehensive numerical modeling for both temperature analysis and thermoelastic or thermoplastic analysis. While it is possible to perform a full-scale, three-dimensional finite element analysis of the welding problem, the computational cost can be enormous. As an alternative, the residual stress field can be specified directly from a suitable experimental database. The database, which might have been developed for a set of specific conditions, is sometimes difficult to apply because of the need to extrapolate to other cases of interest. Nevertheless, this approach can be valuable for prescribing weld residual stresses. It is discussed in the next section.

5.2. Residual stress field in a pipe weld

There is significant residual stress variation from weldment-to-weldment even for large-diameter pipes. Substantial effort has been made in the past to calculate and/or experimentally measure the magnitude and distribution of residual stresses in austenitic pipe welds [25–31].

Fig. 19 shows the available experimental data for the axial residual stress in large diameter pipes as a function of radial distance into the pipe wall from the inside surface [26–32]. Few experimental measurements of circumferential through-wall residual stress distributions have been reported. Fig. 20 shows the data available for circumferential, inside surface residual stress as a function of pipe diameter. Inside surface measurements on 101.6 mm (4 inch) to 304.8 mm (12 inch) pipe weldments with smaller wall thicknesses show that the circumferential residual stresses are tensile and are similar in magnitude to the axial residual stresses [25,33]. The data in Fig. 20 and finite element calculations presented in [27] and [29] suggest that the circumferential stresses on the inner surface of large-diameter (diameter $\geq$405.4 mm [16 inch]) pipe-to-pipe weldments that are thicker can become compressive,

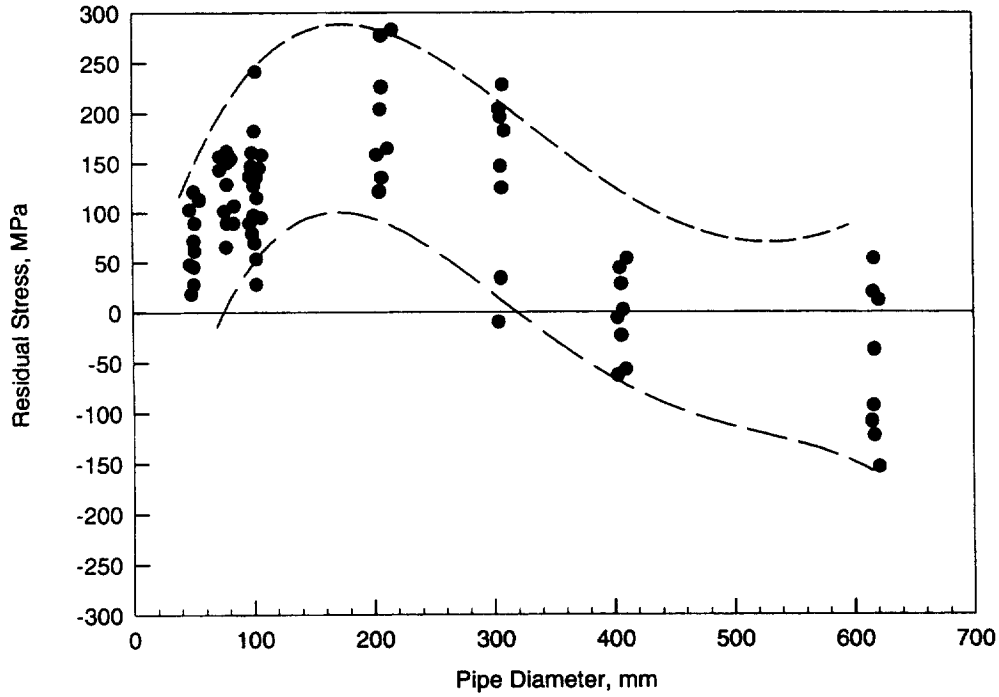

Fig. 20. Circumferential residual weld stress in heat-affected zone at the inside surface of the pipe as a function of diameter of Schedule 80 pipe.

Table 4
Prescribed residual stress field from ASME Section XI IWB-3640 analyses

Wall thickness	Through-wall residual stress[a] Circumferential	Axial
$t = 8.9$ mm	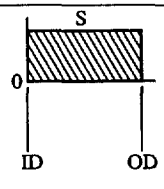	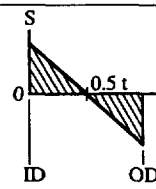
$t = 26.41$ mm	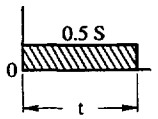	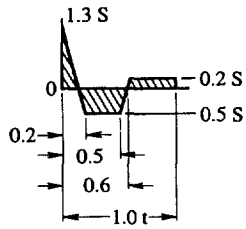

[a]S = 207 MPa (30 ksi).

although this may depend on the heat input during fabrication.

Finite element calculations, [27,29] supported by limited experimental measurements [25,26] suggest that there are significant differences in through-wall residual stress distributions between thinner-wall small-diameter (i.e. less than 102 mm [4.0 inch]) and thicker-wall large-diameter (i.e greater than 406 mm [16 inch]) pipe weldments. The calculations also suggest that the form of the stress distributions in intermediate thickness and diameter (254 mm [10 inch] to 305 mm [12 inches) weldments depends strongly on the weld heat input [29]. The residual stress differences are due primarily to the increased heat capacity of thicker-wall pipe and are only coincidentally associated with the diameter. Consequently, the recommended residual stresses are given in terms of wall thickness with a transition chosen somewhat arbitrarily at 25.4 mm (1 inch).

Based on the available data and FEM computations, the axial and circumferential through-wall residual stress distributions recommended by the Task Group on Piping Flaw Evaluation of ASME section XI are presented in Table 4 [34]. Because there is a lack of data, through-thickness uniform axisymmetric distributions were recommended for the circumferential through-wall residual stresses.

Pipe-to-pipe welds represent only a portion of the welds in nuclear power plants. Little experimental data is available for other configurations. However, finite element calculations have been carried out for a variety of weld geometries including a 304.8 mm (12 inch) pipe-to-sweepolet weld, a 304.8 mm (12 inch) pipe-to-reducer weld, and a 558.8 mm (22 inch) pipe-to-valve weld. In all three cases the weld induced axial stresses are compressive, and an upper bound of stress distribution is shown in Table 4. The stress field given in Table 4 was used in this study to evaluate the effects of the residual stresses on the crack-opening-area analysis.

5.3. Applications of residual stresses for COA analysis

Once the residual stress field is calculated from a numerical analysis, or defined from an experimental database, the pipe flaw evaluation can be performed to study the effects of residual stress on crack-opening characteristics. Ideally, one can apply the residual stresses as "initial" locked-in stresses and then introduce a through-wall-crack to conduct crack-opening-area analysis. In this way, the redistribution of stresses that occurs due to the presence of the crack can be automatically accounted for in the subsequent finite element analysis.

In this study, a simpler alternative approach [35] was undertaken. In this approach, the residual stresses were applied as crack-face pressure since the superposition principle is applicable for linear-elastic stress analysis,The stresses were applied as force-controlled as for a very long pipe far from restraints. The superposition principle implies that the state of stress due to two or more loads acting together is equal to the sum of the stresses due to each load acting separately. The redistribution of stresses that occurs due to the presence of the crack, growing or non-growing, does not imply that the superposition principle is invalid. This fact has been pointed out by Parker [36] for fatigue crack growth and demonstrated by Quinones and Reaugh [37] for stress corrosion crack growth. Also, in the present work, no circumferential residual stresses were applied for the circumferential crack since they would have negligible effects in a linear-elastic analysis [35].

5.4. The pipe crack problem

In this analysis a through-wall-cracked pipe was used

Table 5
Geometric details and applied bending moments for large and small diameter pipes used in finite element analysis.

Pipe	Outer diameter (mm)(inch)	Wall thickness (mm)(inch)	θ/π (%)	Bending moment (kNm)
Thicker-wall, large-diameter pipe	402.6 (15.85)	26.41 (1.04)	12	522.07(*)
Thinner-wall, small-diameter pipe	102.0 (4.02)	8.9 (0.35)	20	8.83(†)

(*) The corresponding elastic stress = 189.4 MPa (1.08 × ASME service level A limit).
(†) The corresponding elastic stress = 158.23 MPa (0.9 × ASME service level A limit).

with outer diameter, D_o and wall thickness, t. Two pipes were chosen, one with large diameter and thickness, e.g. $D_o = 402.6$ mm (15.85 inches) and $t = 26.41$ mm (1.04 inches), the other with small diameter and thickness, e.g. $D_o = 102.0$ mm (4.02 inches) and $t = 8.9$ mm (0.35 inch). The pipe has a circumferential through-wall crack with total crack angle, 2θ. The pipe and crack geometries are defined in Table 5. The crack sizes were small enough to be representative of typical situations encountered in leak-before-break analyses. In both pipes, the cracks are symmetrically located on the bending plane and have the same length on the inside diameter and the outside diameter in terms of percentage of pipe circumference.

In both pipes, the material was TP304 stainless steel at 288°C (550 F). The modulus of elasticity and Poisson's ratio were assumed to be 193.06 GPa (28 000 ksi) and 0.3, respectively. The design stress intensity, S_m, defined by Section II of the ASME code [38] is 116.9 MPa (16.95 ksi) at 288°C (550 F). However, since this is an elastic analysis, the results should be applicable to ferritic welds, assuming they have a similar residual stress field. The residual stress distributions in Table 4 came from experimental work on stainless steel welds, as mentioned previously.

For this study, both pipes were unpressurized and were subjected to pure bending moments applied at the remote ends. The moments were 522.1 kNm (4621 inch-kip) and 8.83 kNm (78.16 inch-kip) for the thicker-wall large-diameter and thinner-wall small-diameter pipes, respectively, see Table 5. These moments correspond to elastic bending stresses (at the outer fiber of uncracked pipe cross-section) of 189.4 MPa (27.47 ksi) and 158.23 Mpa (22.95 ksi) for the thicker-wall large-diameter and thinner-wall small-diameter pipes, respectively. These stresses were larger than typical normal operating stresses (axial plus bending combined) in a nuclear plant piping. Comparisons with the ASME Service Level A stress limit, which is defined as 1.5 S_m show that the above stresses correspond to 1.08 and 0.9 times the Service Level A stresses, respectively. However, since the analysis is linear-elastic, the COD results can be linearly scaled for any given applied moment or stress. Scaled COD results are discussed in a forthcoming section.

For the crack-opening-area analyses, two different load cases were considered. In the first case, the above bending load was applied without any residual stresses. In the second case, the bending load was applied with the residual stresses prescribed in Table 4. In both cases the loadings were assumed to be elastic, so there was no plasticity and/or crack growth. This was justified since normal operating stresses associated with a leaking crack are typically elastic.

5.5. Finite element analysis

5.5.1. Results of analysis

Linear-elastic finite element analyses were conducted to determine the crack-opening for each pipe with the two load cases defined above. The general-purpose commercial code ABAQUS [16] was used in the analyses. The finite element idealizations involved 3200 20-noded three-dimensional solid elements. The number of elements through the thickness was ten. Due to symmetry in both the longitudinal and circumferential directions, only one-quarter of the pipe was modeled. Fig. 21 shows the original (undeformed) finite element mesh for one of the pipes.

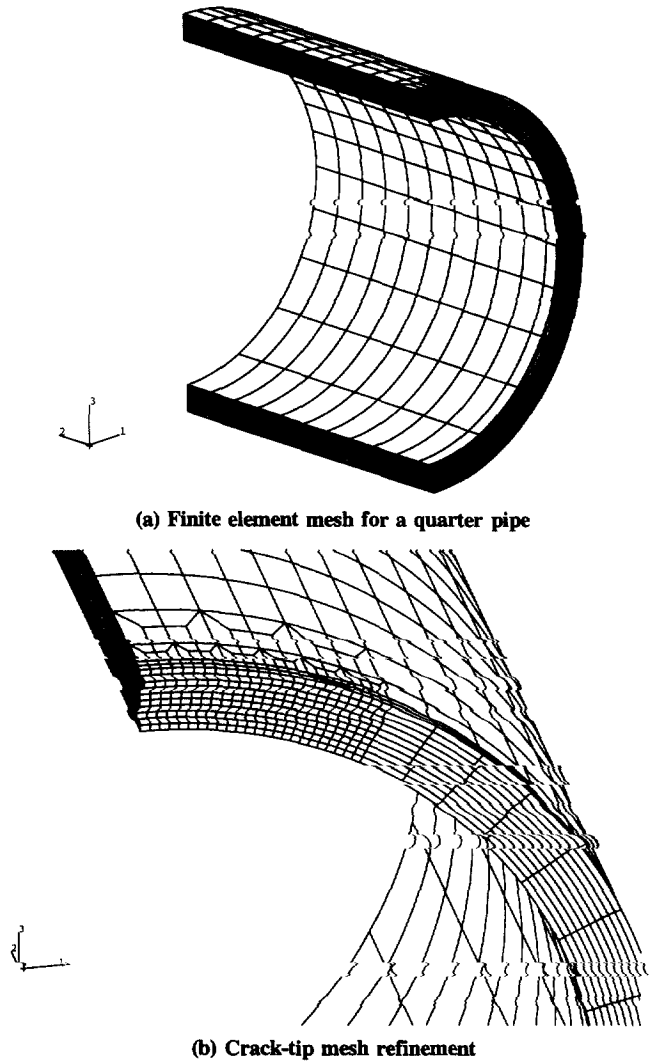

(a) Finite element mesh for a quarter pipe

(b) Crack-tip mesh refinement

Fig. 21. Finite element model for residual stress analysis: (a) finite element mesh for one-quarter pipe; (b) crack-tip mesh refinement.

Table 6 shows the predicted values of center COD at the inside, middle, and outside surfaces calculated by the finite element analyses with and without residual stresses. The results indicate that the center-crack-opening-displacement at the inside and the outside surfaces could be increased or decreased due to the inclusion of residual stresses. Also, the prescribed residual stress field, defined by Table 4, did not significantly affect the crack-opening for the large-diameter pipe ($D_o = 402.6$ mm [15.85 inch]), but could seriously affect the crack-opening for small-diameter

Table 6
Center-crack-opening displacements calculated with and without residual stresses from finite element analysis

Pipe	Outer diameter (mm)	Load case	Center-crack-opening displacement (mm) Inside surface	Middle surface	Outside surface
Thicker-wall, large-diameter pipe	402.6	Bending moment(*) only	0.274	0.334	0.395
		Bending moment(*) and residual stress	0.286 (+4.4)(†)	0.326 (−2.4)(†)	0.408 (+3.3)(†)
Thinner-wall, small-diameter pipe	102.0	Bending moment(‡) only	0.111	0.137	0.164
		Bending moment(‡) and residual stress	0.130 (+17.1)(†)	0.121 (−11.7)(†)	0.112 (−31.7)(†)

(*) Moment = 522.07 kNm with corresponding elastic stress = 189.4 MPa (1.08 × ASME service level A limit).
(†) Percent change relative to center COD calculated without residual stress (+ = increase, − = decrease).
(‡) Moment = 8.83 kNm with corresponding elastic stress = 158.23 MPa (0.9 × ASME service level A limit).

pipes (D_o = 102.0 mm [4.02 inch]). More specifically, for the large-diameter pipe, when the residual stresses were considered, the center-crack-opening displacement increased by 4.4% at the inside surface, decreased by 2.4% at the middle surface, and increased by 3.3% at the outer surface of the pipe. For the small-diameter pipe, when the residual stresses were included, the center COD at the inside, middle, and outside surfaces increased by 17.1%, decreased by 11.7%, and decreased by 31.7%, respectively.

More detailed results related to the effects of the above residual stresses are provided in Figs 22 and 23, which show the plots of center COD as a function of a normalized distance, u/t, where u is the coordinate distance (radial) from the inside surface of the pipe and t is the pipe wall thickness. The functional variation of center COD with respect to u/t was calculated with and without residual stresses for both the thicker-wall large-diameter pipe and the thinner-wall small-diameter pipe and are shown in Figs 22 and 23, respectively. The analyses indicate that the effects of residual stresses for the thinner-wall pipe are significantly greater than those for the thicker-wall pipe.

5.5.2. *Effects of residual stresses for various applied loads*

At more typical normal operating stresses, which can be much smaller than the applied stresses used in these analyses, the effects of residual stresses on crack-opening can be much higher. Since the analyses performed in this study are linear-elastic, the effects of residual stresses for pipes with any other applied loads can also be evaluated. This is because the results of FEA conducted for the applied moments in Table 5, can be sealed linearly for any other moments or stresses.

Based on linear scaling, Figs 24 and 25 show the percent change in center COD due to the inclusion of residual stresses for both thicker-wall large-diameter and thinner-wall small-diameter pipes, respectively. In both figures, the horizontal axis defines the applied moment that corresponds to an applied elastic stress as a percentage of ASME Service Level A stress limits. The vertical axis represents the difference of the calculated center COD with residual stresses (δ_{M+RS}) and without residual stresses (δ_M) normalized by the center COD without residual stresses. In general, the effects of residual stresses are significant when the normal operating stresses are lower. For example, when the applied stress is equal to 50% of ASME Service Level A stress, the center COD for the thick-walled large diameter pipe will increase by 9.46 and 7.11% at the inside and outside surfaces, respectively, and decrease by 5.17% at the mid-thickness level. Correspondingly, the center COD for the thin-walled small-diameter pipe will increase by 30.9% at the inner surface

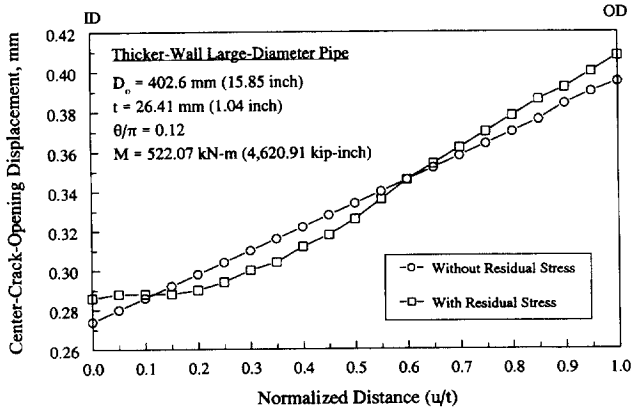

Fig. 22. Effects of residual stresses on the through-the-thickness variation of center-crack-opening displacement for the thick-walled large-diameter pipe.

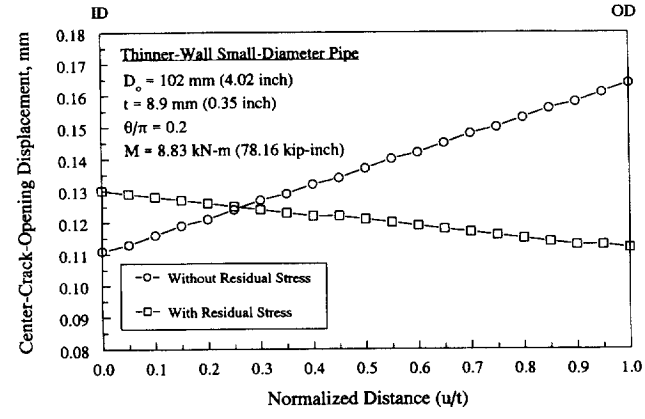

Fig. 23. Effects of residual stresses on the through-the-thickness variation of center-crack-opening displacement for the thin-walled small-diameter pipe.

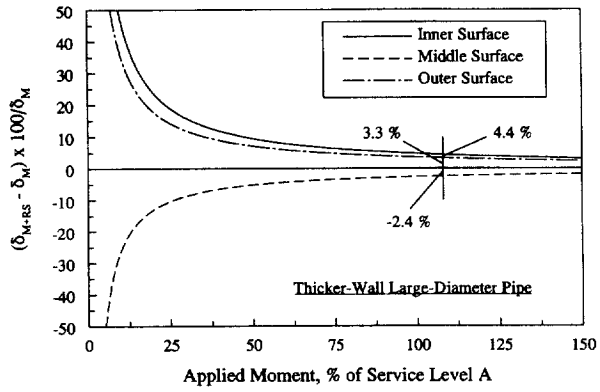

Fig. 24. Percentage change in calculated COD due to residual stress as a function of applied moment for the thick-walled large-diameter pipe.

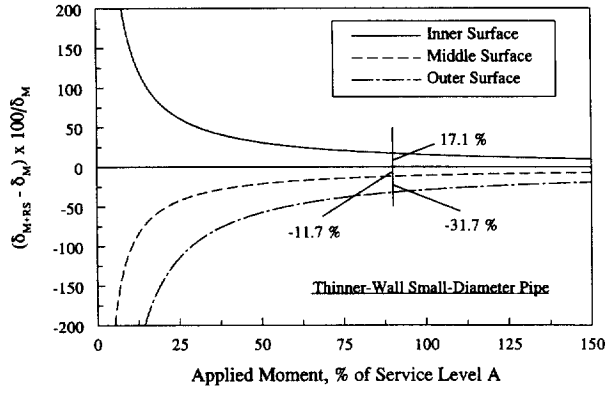

Fig. 25. Percentage change in calculated COD due to residual stress as a function of applied moment for the thin-walled small-diameter pipe.

and decrease by 57.2 and 21.1% at the outer and middle surfaces of the pipe, respectively. Relative comparisons of the crack-opening results in Figs 24 and 25 indicate that at any given applied load the residual stress effects are more severe for the thin-walled small-diameter pipe than for the thick-walled large-diameter pipe.

According to Fig. 24, for the thick-walled large-diameter pipe, the calculated CODs which account for residual stresses are always larger than those estimated without residual stresses at both inner and outer surfaces of the pipe. However, the COD at the mid-thickness level can be smaller when the residual stresses are considered. For the thin-walled small-diameter pipe, the results for which are shown in Fig. 25, the calculated COD with residual stresses are higher at the inner surface and lower at the outer or middle surfaces than those without residual stresses. Consequently, the crack-opening area and the subsequent leak-rate calculations can be affected by the residual stresses in those pipes. In particular, when the values of δ_{M+RS} and δ_M are such that $(\delta_{M+RS} - \delta_M) \times 100/\delta_M$ (the variable in the vertical axis) reaches a value of -100, the calculated center COD with residual stresses becomes zero. Hence, there would be no leakage even for a pipe containing a through-wall crack, which clearly demonstrates how important the residual stresses are for the leak-rate calculations. This is especially true for the thin-walled small-diameter pipe in which case the results in Fig. 25 predict that due to the residual stress, the outer surface of the pipe will close (thus preventing any leakage) when the applied load is equal to 28.6% of the ASME Service Level A stress limit. Similar calculations can also be made for the middle surface of both pipes, but the trend curves in Figs 24 and 25 suggest that for closure to occur, the applied stresses would have to be very small, i.e. 2.60 and 10.5% of the ASME Service Level A stress limit for the thicker-wall large-diameter and thinner-wall small-diameter pipes, respectively.

Finally, the above results of COD should be viewed as the preliminary estimates for the residual stress effects. No efforts were undertaken to determine the accuracy of this approximate finite element analysis compared with more rigorous thermoplastic finite element analysis, where the residual stress field is numerically simulated. One major difference between these two approaches, is that modeling the residual stress field as a crack-face pressure, imposes a load-controlled stress field, whereas, the actual residual stresses are a local displacement-controlled stress field. The load-controlled crack-face-pressure modeling should produce a larger effect on the COD, than the thermo-plastic modeling of the residual stresses (with unpinning of the nodes to determine the COD). Considering these aspects, the results from this analysis should overemphasize predictions of the crack-opening displacements due to residual stresses. Nevertheless, the conclusion that the residual stress effects on the COD for thinner-wall small-diameter pipe are more severe than the thicker-wall large-diameter pipe, is an important result.

6. Conclusions

Based on the results from this study, the following conclusions can be drawn:

- The crack-opening area for a pipe with an off-centered crack can be determined by normal analysis procedures for a centered crack by resolving the applied moment to the effective moment at the center of the off-centered crack and assuming an elliptical profile for the crack-opening shape. This was an important finding since for leak-rate calculations, accuracy in the prediction of crack-opening area is more significant than that of the entire crack-opening shape.
- The restraint of the induced bending due to an axial (pressure) tension increases the failure stresses, but can decrease the crack-opening at a given load. If the pipe system restrains the bending (i.e. from cracks being close to a nozzle or restraint from the rest of the piping system), then the actual leak rate would be less than the leak rate calculated by using analyses that assume that

the pipe is free to rotate. This will cause the actual leakage crack size to be larger than calculated by the current analysis methods for the same leak rate. When the crack angle is small ($\theta/\pi \leq 1/8$), the restraint effects are also small and may be neglected. However, for larger crack angles ($\theta/\pi \geq 1/4$), the crack-opening displacement for the case where the induced bending is restrained could be significantly smaller than the crack-opening displacement for the unrestrained condition. Hence, the restraint effects should not be ignored in the crack-opening and leak-rate analyses, particularly for small-diameter pipes where the leaking crack size could be large for typical plant stresses and leakage detection requirements.

- Due to thickness gradients on both sides of the crack, the component of crack-opening displacement in the thinner side of the crack is much larger than that in the thicker side, thereby breaking the symmetry of the crack-opening shape with respect to the crack length. The differences in these components can be significant when the applied moment is large to induce plasticity.
- The prescribed residual stress field from ASME Section XI technical basis document IWB-3640 affected the crack-opening for the thicker-wall large-diameter pipe much less than that for the thinner-wall small-diameter pipe. For the large-diameter pipe with residual stresses and an applied moment yielding a bending stress of 0.5 times the ASME Service Level A stress limit, the center-crack-opening displacement:

  increased by 9.46% at the inside surface,
  decreased by 5.17% at the middle surface, and
  increased by 7.11% at the outer surface of the pipe.

- For the small-diameter pipe when the residual stresses were included with an applied moment giving a bending stress of 0.5 times the ASME Service Level A limit, the center-crack-opening displacement:

  increased by 30.9% at the inside surface,
  decreased by 57.2% at the mid-thickness, and
  decreased by 21.1% at the outside surface.

- Relative comparisons of the crack-opening results for these two pipes indicate that at any given applied bending stress, the residual stress effects are more severe for the thin-walled small-diameter pipe than for the thick-walled large-diameter pipe. However, this hypothesis needs to be re-evaluated for other types of residual stress field not explicitly considered in this study.
- For both thicker-wall large-diameter pipe and thinner-wall small-diameter pipe, plots of crack-opening displacement vs applied moment showed that at some value of this applied moment, the crack-opening could be zero when residual stresses were included. For the thinner-wall small-diameter pipe, the analysis predicted that due to the residual stress, the outer surface of the pipe would close (thus prevent any leakage) when the applied load was equal to 28.6% of the ASME Service Level A stress limit. Similar calculations could also be made for the middle surface of both pipes, but the trends in the results suggest that for closure to occur, the applied stresses would have to be very small, i.e. 2.60 and 10.5% of the ASME Service Level A stress limit for the thicker-wall large-diameter and thinner-wall small-diameter pipes, respectively.
- The finite element modeling in the residual stress analyses conducted in this work probably overpredicts their significance on the crack-opening because of the modelling technique used. This analysis applied the residual stress field as a load-controlled crack face pressure, whereas the residual stresses are strain induced over the weld region. A more sophisticated finite element analysis (e.g. a thermoplastic analysis) is needed to account for these effects.

Acknowledgements

The authors would like to thank Mr Michael Mayfield and the US NRC Office of Research, Electrical, Materials, and Mechanical Engineering Branch for their encouragement and support of this effort as part of the US NRC's 'Short Cracks in Piping and Piping Welds' program, Contract No. NRC-04-90-069. Their support and guidance are sincerely appreciated. The authors would also like to thank Dr Y-H. Choi of Korea Institute of Nuclear Safety for obtaining measurements of nozzle geometry and Mr T. Kilinski of Battelle for developing some plots.

References

[1] Rahman S, Brust FW, Ghadiali N and Wilkowski G. Crack-opening-area analyses for circumferential through-wall cracks in pipes—Part I: analytical models. *International Journal of Pressure Vessels and Piping*, 1998;75:357–373.

[2] Rahman S, Brust FW, Ghadiali N and Wilkowski G. Crack-opening-area analyses for circumferential through-wall cracks in pipes—Part II: model validations. *International Journal of Pressure Vessels and Piping*, 1998;75:375–396.

[3] Rahman S, Brust F, Ghadiali N, Choi YH, Krishnaswamy P, Moberg F, Brickstad B and Wilkowski G. Refinement and evaluation of crack-opening-area analyses for circumferential through-wall cracks in pipes. NUREG/CR-6300, US Nuclear Regulatory Commission, Washington, D.C., April 1995.

[4] Wilkowski GM, Ahmad J, Barnes CR, Brust F, Ghadiali N, Guerrieri D, Jones D, Kramer G, Landow M, Marschall CW, Olson R, Papaspyropoulos V, Pasupathi V, Rosenfeld M, Scott P and Vieth P. Degraded piping program—Phase II: Summary of technical results and their significance to leak-before-break and in-service flaw acceptance criteria. NUREG/CR-4082, vol. 8, US Nuclear Regulatory Commission, Washington, D.C., March 1989.

[5] Paul D, Ahmad J, Scott PM, Flanigan LF and Wilkowski G. Evaluation and refinement of leak-rate estimation models. NUREG/CR-5128, Rev. 1, US Nuclear Regulatory Commission, Washington, D.C., June 1994.

[6] Wilkowski G, Rahman S, Paul D and Ghadiali N. Pipe fracture evaluations for leak-rate-detection: Deterministic models. *Creep, fatigue evaluation, and leak-before-break assessment*, 1993, 266, 243–254.

[7] Kumar V, German M and Shih C. An engineering approach for elastic–plastic fracture analysis. EPRI Report NP-1931, Electric Power Research Institute, Palo Alto, CA, 1981.

[8] Kumar V, German M, Wilkening W, Andrews W, deLorenzi H and Mowbray D. Advances in elastic–plastic fracture analysis. EPRI Final Report NP-3607, Electric Power Research Institute, Palo Alto, CA, August 1984.

[9] Brust F, Rahman S, Ghadiali N. Elastic-plastic analysis of small cracks in tubes. Journal of Offshore Mechanics and Arctic Engineering, 1995;117(1):57–62.

[10] Klecker R, Brust F and Wilkowski G. NRC leak-before-break (LBB.NRC) analysis method for circumferentially through-wall-cracked pipes under axial plus bending loads. NUREG/CR-4572, US Nuclear Regulatory Commission, Washington D.C., September 1986.

[11] Paris PC and Tada H. The application of fracture proof methods using tearing instability theory to nuclear piping postulating circumferential through-wall cracks. NUREG/CR-3464. US Nuclear Regulatory Commission, Washington, D.C., 1983.

[12] Brust FW. Approximate methods for fracture analyses of through-wall cracked pipes. NUREG/CR-4853, US Nuclear Regulatory Commission, Washington, D.C., February 1987.

[13] Rahman S, Brust F. An estimation method for evaluating energy release rates of circumferential through-wall cracked pipe welds. Engineering Fracture Mechanics (Vol. 43–3), 1992:417–430.

[14] Rahman S, Brust F. Elastic-plastic fracture of circumferential through-wall cracked pipe welds subject to bending. Journal of Pressure Vessel Technology (Vol. 114–4), 1992:410–416.

[15] Wilkowski GM, Brust F, Francini R, Ghadiali N, Kilinski T, Krishnaswamy P, Landow M, Marschall CW, Rahman S and Scott P. Short cracks in piping and piping welds. Semi-annual reports, vols. 1, 2, and 3, nos. 1 and 2. NUREG/CR-4599, US Nuclear Regulatory Commission, Washington, D.C., 1990–1992.

[16] *ABAQUS, Users Guide and Theoretical Manual*, Version 5.3. Hibbitt, Karlsson, and Sorensen, Pawtucket, RI, 1993.

[17] Schmidt RA, Wilkowski GM and Mayfield ME. The international piping integrity research group (IPIRG) program: an overview. *Transactions of the 11th International Conference on Structural Mechanics in Reactor Technology, Vol. G2: fracture mechanics and non-destructive evaluation—2*, Shibata H, editors. Tokyo, Japan, Paper No. G23/1, August 1991, pp. 177–188.

[18] Norris D et al. PICEP: pipe crack evaluation program. EPRI Report NP-3596-SR, Electric Power Research Institute, Palo Alto, CA, 1984.

[19] Barber TE, Brust FW, Mishler HW and Kanninen MF. Controlling residual stresses by heat sink welding. EPRI Report NP-2159-LD, Electric Power Research Institute, Palo Alto, CA, 1981.

[20] Kanninen MF, Brust FW, Ahmad J and Abou-Sayed IS. The numerical simulation of crack growth in weld-induced residual stress fields, *Residual stress and stress relaxation*, Kula E and Weiss V, editors. In *Proceedings of 28th Army Sagamore Research Conference*, Lake Placid, NY, July 1981, 227–248.

[21] Brust FW, Rybicki EF. A computational model of backlay welding for controlling residual stresses in welded pipes. Journal of Pressure Vessel Technology, 1981;103:226–232.

[22] Brust FW, Kanninen MF. Analysis of residual stresses in girth welded type 304 stainless steel pipes. Journal of Materials for Energy Systems, 1981;3(3):56–62.

[23] Iwamura Y and Rybicki EF. A transient elastic–plastic thermal stress analysis of flame forming. *ASME Transactions Journal of Engineering for Industry*, 1973, 163–171.

[24] Klepfer H, et al. Investigation of cause of cracking in austenitic stainless steel piping. General Electric Report No. NEDO-21000-1, July 1975.

[25] Shack WJ, Ellingson WA and Pahis L. Measurement of residual stress in type 304 stainless steel piping butt weldments. EPRI Report NP-1413, Electric Power Research Institute, Palo Alto, CA, 1980.

[26] Shack WJ. Measurement of through-wall residual stresses in large diameter type 304 stainless steel piping butt weldments. Report ANL-82-15, Argonne National Laboratory, Argonne, IL, 1982.

[27] Shack WJ, et al. Environmentally assisted cracking in light water reactors. Annual Report, October 1981 to September 1982, NUREG/CR-3292, US Nuclear Regulatory Commission, Washington, D.C.

[28] Rybicki EF, Schmueser D, Stonesifer R, Groom J and Mishler H. Residual stresses at girth-butt welds in pipes and pressure vessels. NUREG-0376, US Nuclear Regulatory Commission, Washington, D.C., 1977.

[29] Rybicki EF, McGuire P, Shadley J, Koch R and Merah N. Computational residual stress analysis for induction heating of welded BWR pipes. EPRI Report NP-2662-LD, Electric Power Research Institute, Palo Alto, CA, 1982.

[30] Shack WJ, et al. Environmentally assisted cracking in light water reactors. Annual Report, October 1983 to September 1984, NUREG/CR-4287, US Nuclear Regulatory Commission, Washington, D.C., 1985.

[31] Harris DO. The influence of crack growth kinetics and inspection on the integrity of sensitized BWR piping welds. EPRI Report NP-1163, Electric Power Research Institute, Palo Alto, CA, 1979.

[32] Horn RM. The growth and stability of stress corrosion cracks in large diameter BWR piping. EPRI Report, NP-2472, Vols. 1 and 2, Electric Power Research Institute, Palo Alto, CA, July 1982.

[33] Sasaki R, et al. Mitigation of inside surface residual stress of type 304 stainless steel pipe welds by inside water cooling method. In *Proceedings: Seminar on Countermeasures for Pipe Cracking in BWRs*, EPRI WS-79-174, vol. I. Electric Power Research Institute, Palo Alto, CA, 1980.

[34] Evaluation of flaws in austenitic steel piping. (Technical basis document for ASME IWB-3640 analysis procedure), prepared by Section XI Tasl Group for Piping Flaw Evaluation, EPRI Report NP-4690-SR, Electric Power Research Institute, Palo Alto, CA, July, 1986.

[35] Bergman M and Brickstad B. A new computerized procedure to analyze LBB in pipes with complex crack shapes. In *Proceedings of the 20th MPA-Seminar*, Stuttgart, Germany, October 1994.

[36] Parker AP. LEFM and fatigue crack growth residual stress effects. *Residual Stress and Stress Relaxation*, Kula E, editor. Plenum Publication Corporation, 1982, pp. 249–271.

[37] Quinones DF and Reaugh JE. Weld residual stress distribution near growing cracks. EPRI Report NP-2694, Electric Power Research Institute, Palo Alto, CA, 1983.

[38] 1992 ASME Boiler and Pressure Vessel Code—Section II, Materials: Part D—properties.